Supplementary Information

Surface Controlled Pseudo-Capacitive Reactions Enabling Fast Charging and Life Long Organic Lithium Ion Batteries

Kamran Amin[1,2], Jianqi Zhang[1], Zhou Hang Yu[1], Ruichao Lu[1], Miao Zhang[1], Nawal Ashraf [1,2], Cheng YueLi[1], Lijuan Mao[1], Charl F.J. Faul[3], Wei Zhixiang*[1,2]

1. National Center for Nanoscience and Technology, Chinese Academy of Sciences, 11 Zhongguancun North 1st Alley, Haidian Qu, Beijing Shi, China, 100190

2. University of Chinese Academy of Sciences, No.19(A) Yuquan Road, Shijingshan District, Beijing, P.R.China 100049

3. University of Bristol, Beacon House, Queens Road, Bristol BS8 1QU, UK

Materials and Methods:

1,3,5-tris(4-formylphenyl) benzene (TFP) was synthesized according to reported procedure.[1, 2] All other materials were purchased from commercial suppliers and used as received. The suppliers include Alfa Aesar, Merda Technologies, TCI, ACROS ORGANICS and J&K. High purity single walled carbon nanotubes were purchased from TimesNano. The outer diameter was less than 2 nm and purity was greater than 95 % as mentioned by supplier. These CNTs were further washed with water vapors and heat treated at 900 ^{0}C in Ar environment to remove impurities further. Solvent were purchased with extra purity and dried over molecular sieves. Also, solid chemicals were purchased with highest purity level available.

Synthesis:

Synthesis of 1,3,5-tris(4-formylphenyl)benzene (TFP)

In a three necked flask at 25 ^{0}C, hexamethylenetetramine (15.098 g, 108 mmol) and m-trihydroxybenzene (6.014 g, 49 mmol) were added to a solution of 90 mL CF$_3$COOH in a 500 mL under Ar environment. Under continuous stirring this mixture was heated for 1.5 hrs. at 70 ^{0}C. 150 mL of 3M HCL was then added and reaction proceed for 2 more hours at 100 ^{0}C. Reaction mixture was than cooled to room temperature and extracted with 300 ml of dichloro methane. Filtrate was concentrated on rotary evaporator and then washed with hot ethanol to give us a creamy powder with almost 16% of yield. We found that increasing temperature to 100 ^{0}C after adding HCL increases the yield.

H NMR (400 MHz, CDCl3): δ 14.12 (s, 3H, OH), 10.16 (s, 3H, CHO) ppm.

Synthesis of AQ COF

In the first attempt the AQ COF has been synthesized as reported earlier.[1, 3] DAAQ and TFP monomers were added into a glass ampule containing mixture of DMAc and Mesitylene in suitable ratios. The mixture was than sonicated for 20 minutes in bath sonicator and 6M of acetic acid was than added. The ampule was than vacuumed sealed after freeze pump thaw cycle thrice and placed in an oven undisturbed for three days. After 72 hrs the tube was broken to get the material which was washed using 30 ml of DMF 5 times and solvent exchanged with 30 ml of acetone twice. Obtained material was then placed in a vacuum oven at 1800C for 24 hrs. This product was then used for further characterization. The yield was found about 80%.

Synthesis of AQ COF at different conditions

For comparative study three different reaction chamber were chosen. Usually COFs are being synthesized in vacuum sealed glass ampules after three freeze pump thaw cycle. That is a laborious process as well as not easy to upgrade for large scale synthesis. We tried to compare that complicated method with well-established synthesis method. Keeping all the conditions same, in

an attempt lab grade autoclave was used and product is named as AQ COF-A. In second attempt three neck round bottom flask was used with a magnetic stirrer. This reaction was performed under Ar environment. The other conditions were same and product was named as AQ COF-F and in third attempt vacuum sealed glass tube was used and product was named as AQ COF-T. Once comparing the structural characterization, we found that all three obtained products are quite similar to each other and also the electrochemical performance has no significant difference we used AQ COF-F in most our studies except mentioned otherwise.

Solid State NMR: δ 108 s, 118 w, 123w, 129 s, 135s, 144s 181 m, ppm

FTIR: 1658w, 1615w, 1555s, 1240s, 1080, 972m, 890s,813m, 744m, 572, 496 cm^{-1}

AQ COF@CNTs composite synthesis:

AQ-COF@CNTs composite was obtained following an in-situ polymerization process. In another report [4] we already compared the results of making composites with conductive additives through different processes and have concluded that in situ process is best to obtain the comparatively better electrochemical performance. CNTs are being used as conductive backbone and to provide structural strength during the fast charging discharging process.

  CNTs were sonicated with DAAQ in ethanol for one hour and then dried at 50^{0}C under vacuum get a well dispersed CNTs/DAAQ powder. This was then transferred to reaction container along with TFP and solvents were added. Further reaction was proceed as mentioned above. CNTs amount was calculated based on total mass of reactants for example 15 % CNTs means that a mixture of reactants before reaction (DAAQ,TFP and CNTs) contain 15% of CNTs (by weight) in it. Composite with 3 %, 7%, 15% and 20 % of CNTs were obtained through this method and characterized further.

Material Characterization:

Small angle X-ray scattering, XEUSS WAXS/SAXS system, Xenocs, France system was employed with Wavelength 1.54 Å, sample to detector distance is 127.5 mm to study the low angle X-ray Diffraction. SEM SU8200 model was used to get SEM images whereas Hitachi T20 machine was used to get TEM images. AVANCE III HD 400 instrument was used to record HNMR whereas JNM-ECZ600R spectrometer was used to analyze solid state 13C NMR with a mass frequency of 12kHz and relaxation density of 3s. Fourier transform infrared attenuated total reflection (FTIR-ATR) spectra were recorded in the range 400-4000 cm-1 on Spectrum One Perkin-Elmer. Micromeritics ASAP 2420 Accelerated Surface Area and Porosimeter System was used to analyze the BET surface area and pore size distribution.
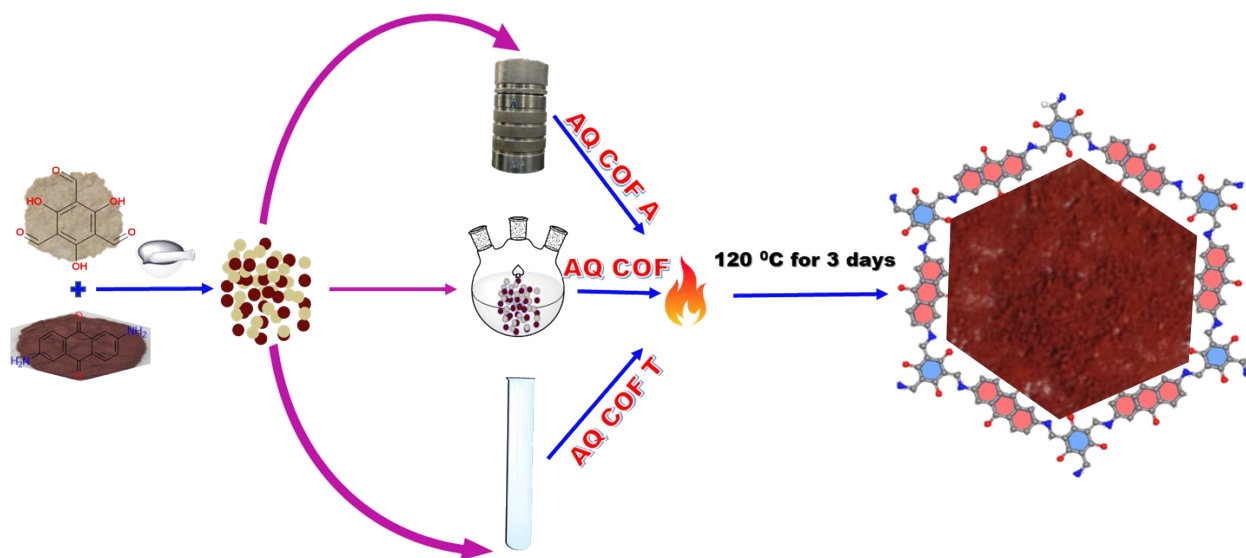

Figure S1: A schematic illustration of synthesis of COF at different conditions. Different reaction vials were employed to synthesize the COF. Since the traditional method of synthesizing COF is expensive, dangerous and cumbersome too. We wanted to develop a method commercially viable for large scale production as well as easy to handle without need of special preparations. So we try 3 different methods. The products are named as AQ-COF, AQ-COF A and AQ-COF-T.
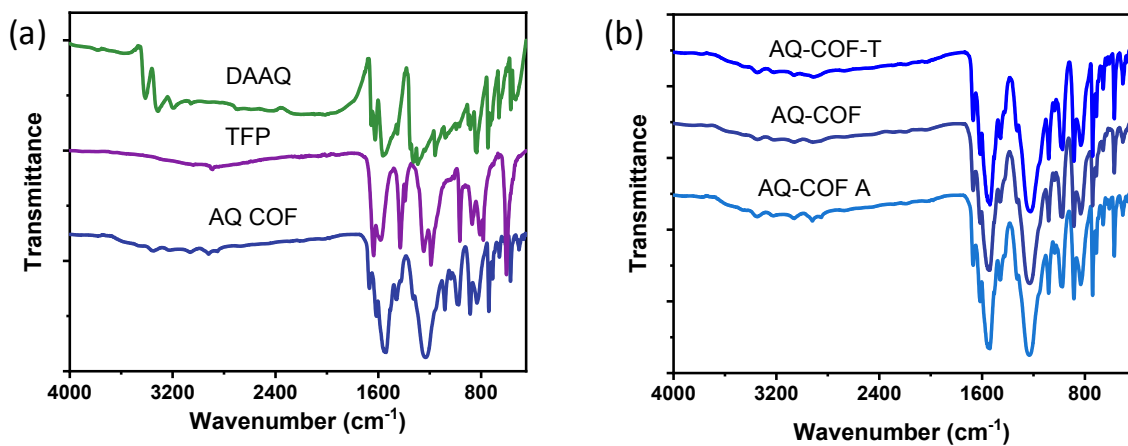
Figure S2: FITR-ATR spectra of (a) AQ COF with monomers and (b) AQ COF synthesized at different conditions. The carbonyl peaks from both monomers can be easily observed in figure S2 (a). Also, the NH peaks from DAAQ monomer completely disappeared in the product. The peaks of COF synthesized at different conditions are completely overlapping suggesting that we have similar product in each case.
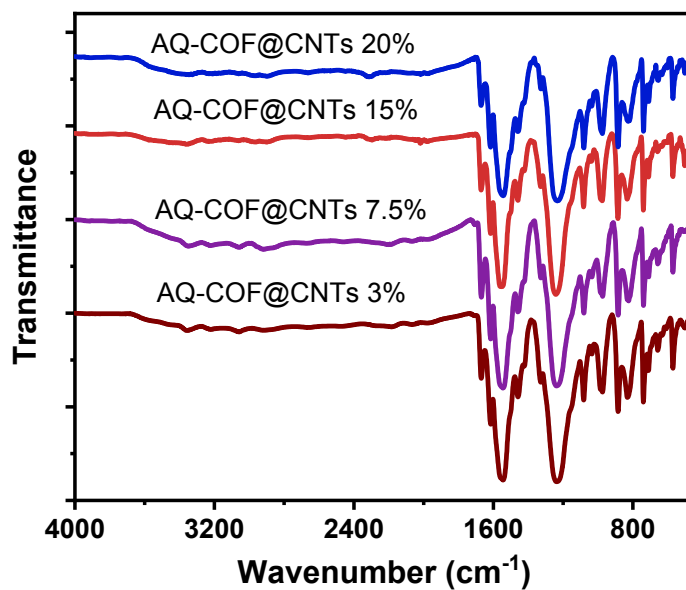
Figure S3: FITR Spectrum of AQ COF grown at CNTs with varying initial percentage of CNTs in the composite. In each case the peaks are completely overlapping suggesting the similar products
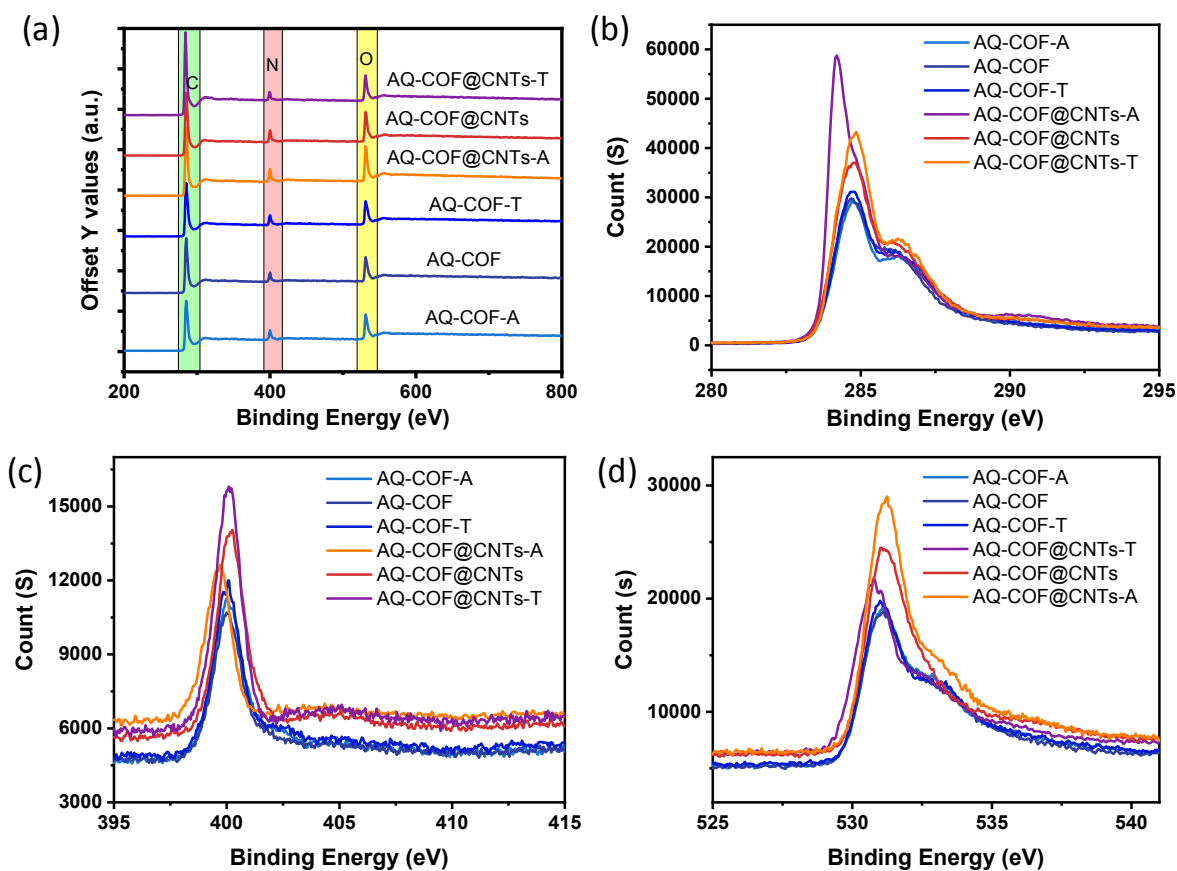
Figure S4: XPS spectra of COF obtained at different conditions. (a) whole elemental scan, (b) carbon C1 (c) N1 and (d) O1 scan. The peaks are occurring at same positions suggesting the similar environment and bonding for all samples.
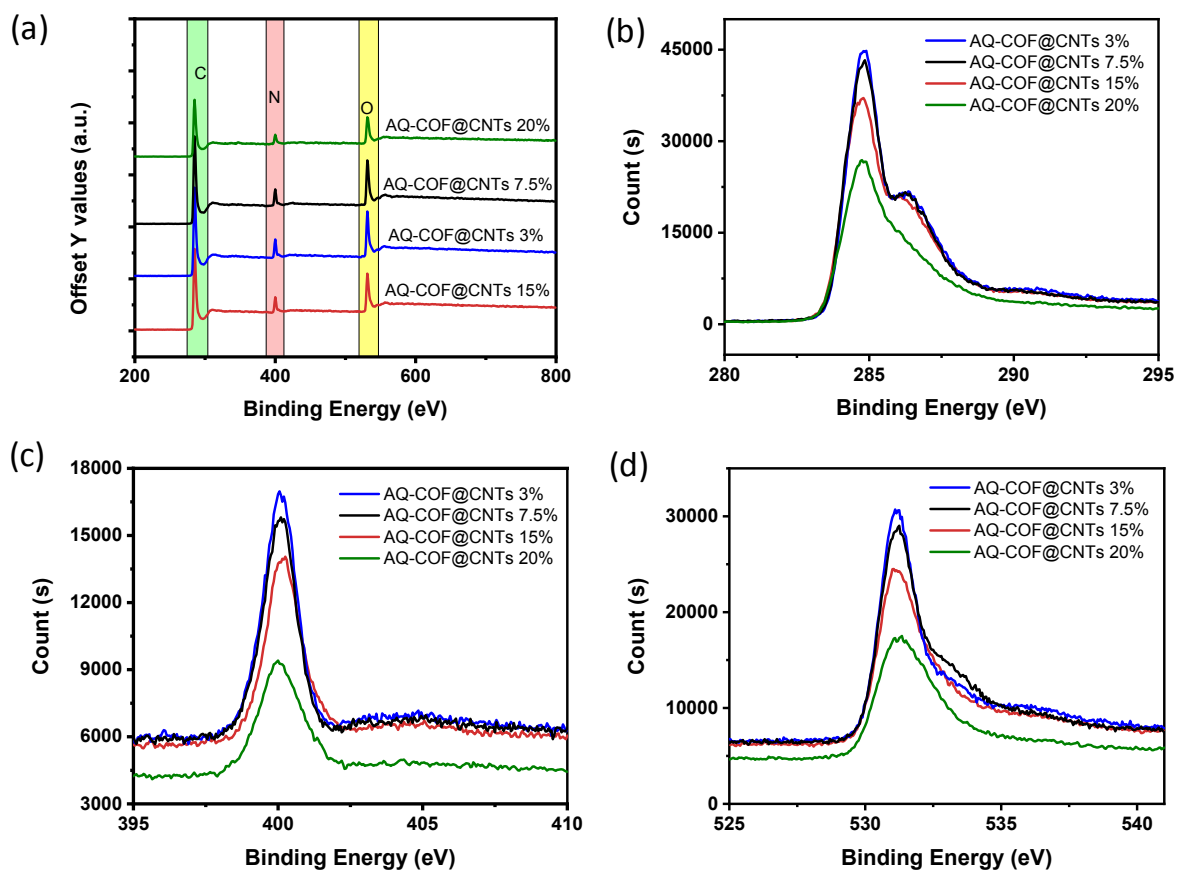
Figure S5: XPS spectra of COF obtained at different CNTs ratios (a) whole elemental scan, (b) carbon C1 (c) N1 and (d) O1 scan. The peaks are occurring at same positions suggesting the similar environment and bonding for all samples.
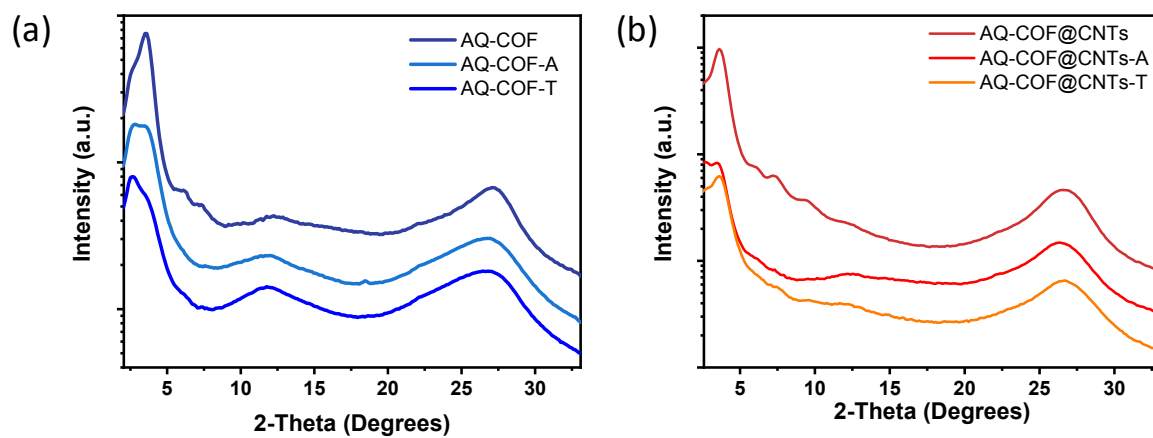
Figure S6: Low angle XRD spectrum of products at different conditions. (a) bare product and (b) product grown on CNTs. The data was plotted against logarithmic graph to highlight the low intensity peaks.

From all these structural characterizations it is quite evident that in each case the obtained product is same irrespective of the conditions used. There may be some difference in crystallinity as it is clear from the XRD but our main focus is on electrochemical performance in this paper. Since the electrochemical performance was also the same as discuss in next sections, we used AQ-COF conditions in most of our product. Since this is a simple method, do not need any special precautions or preparations and easy for scale up production.
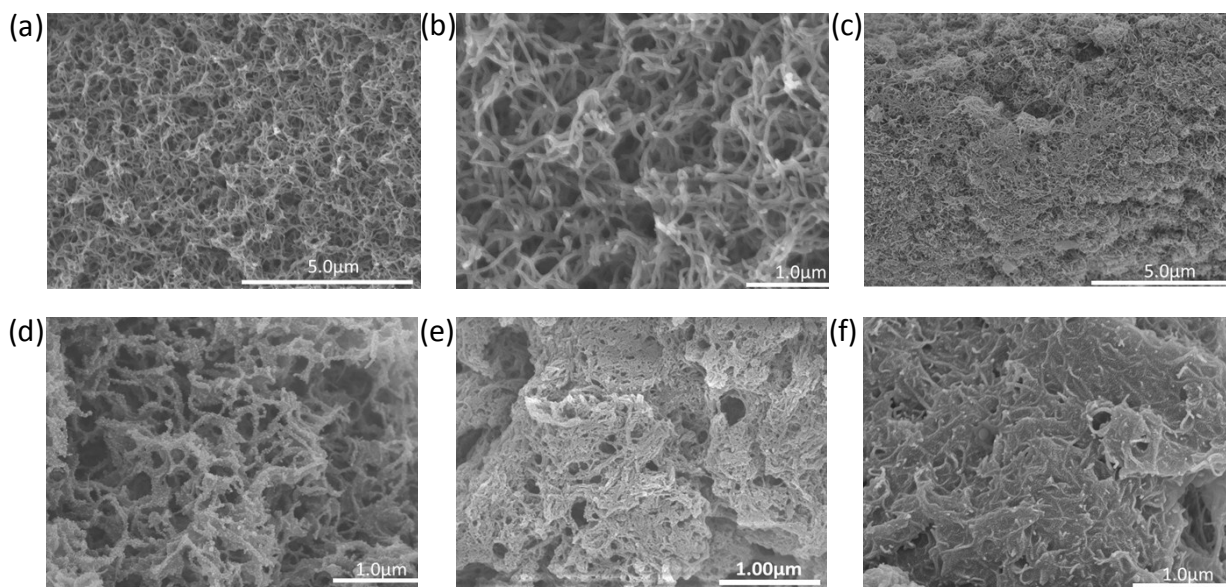
Figure S7: Low- and high-resolution images of (a), (b) AQ COF and (c), (d) AQ COF@CNTs. Also, it can be seen (e), (f) that how nanowires of AQ COF tend to arrange themselves into the sheet like structure.
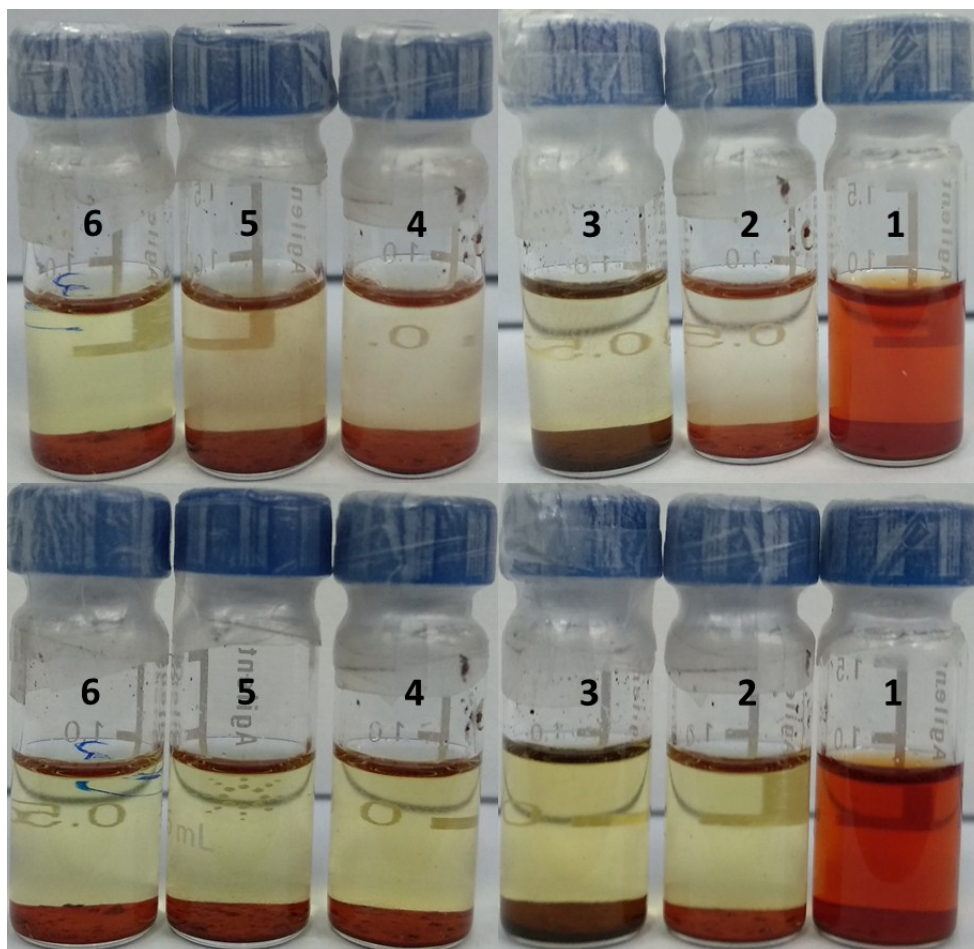
Figure S8: Stability of AQ COF in common electrolytes, 1, DAAQ Monomer, 2 AQ COF, 3 AQ COF@CNTs dissolved in IM LiTFSI in TEGDME. 4 ,5 and 6 AQ COF in LiTFSI in EC:DMC (1:1), 1M LiTFSI dissolved in DME:DOL (1:1), 1M LiPF6 in EC:DEC (1:1) respectively. The image on the top is soon after adding the material in the electrolyte and the image at the bottom is after two months. The concentration of each sample was 2 mg in 1ml of solvent.

Electrochemical Measurement

CR2032 type cell were assembled to measure all the electrochemical properties. AQ COF and AQ COF@CNTs were set as active materials. In case of AQ COF@CNTs the mass including CNTs were taken as active material mass. To prepare the cathode, active material combine with conductive carbon (Super P) and polyvinylidene fluoride (PVDF) binder in a ratio of 6:3:1 were

grind together in mortar and pestle. The CNTs in the composite AQ COF@CNTs are being considered as active material too. A slurry was prepared by adding suitable amount of N-methyl-2-pyrrolidinone (NMP). The slurry was coated on Al foil to prepare the cathode which after drying at 80 ^{0}C under vacuum overnight was cut into the round pieces of 11 mm diameter. Cell was than assembled in argon filled glove box using this cathode along with lithium foil of 16 mm diameter as anode. Celgard 2400 membrane was used as separator and LiTFSI electrolyte (1M) in tetraethylene glycol dimethyl ether (TEGDME) as electrolyte. This electrolyte was recently reported by Wang et al.[1] Rate performance, Galvano-static charge discharge performance and cyclic performance was recorded using the Arbin instruments testing system (Arbin-SCTS) in a potential range of 1.5-3.5V. Cyclic voltammetry (CV) and electrochemical impedance spectroscopy (EIS) measurements were both conducted on an electrochemical workstation, VMP3 Potentiostat/Galvanostat (EG&G, Princeton Applied Research) using the same coin type cells under the potential range of 1.5-3.5V. In sweep rate studies the potential range was set as 1.6-3.2 V to save the time. For EIS tests, the voltage amplitude was 10 mV and the frequency range were 100000 Hz–0.01 Hz and EIS was performed on as synthesize cells. All the electrochemical tests were performed at room temperature.

A comparison of rate performance of AQ COF synthesized at different conditions can be seen on (**Figure S10a**). Almost similar initial capacity as well as rate performance was observed in each case. Also, the effect of CNTs concentration on rate performance was evaluated. Under same conditions the active material utilization is comparative low for 3% and 7.5 % CNTs so as the rate performance (**Figure 4c and S10b**). This is due to the insufficient amount of CNTs to form an effective conductive network in the presence of active material **(Figure 3b)**. Although the rate performance in case 20% CNTs has been improved but the capacity is low compared with 15%

CNTs. This is due to the oversaturation of CNTs in the composite (**Figure 3d, 4c and S10b)**. So we conclude that AQ COF@CNTs with 15% of CNTs delivered the best capacity and better rate performance among all other candidates. Similarly, the effect of synthesis conditions was also investigated for AQ COF@CNTs. AQ COF@CNTs-F exhibited the much better rate performance than AQ COF@CNTs-T. When observed under SEM **(Figure 3c and S11)**, we found that AQ COF@CNTs- F has more or less uniform morphology where CNTs are completely coated with active material and dispersion of CNTs is almost uniform to form an effective interpenetrative conductive network but in case of AQ COF@CNTS-T large isolated material aggregates and CNTs bundles were found. We believe that constant stirring while heating in case of AQ COF@CNTs-F is the main reason for this difference which helps to disperse the matrices into each other effectively while in other case there is no stirring involved and tube is placed undisturbed in oven for three days making it easy for material and CNTs to settle down isolated. So, in our study we used AQ COF@CNTs-F with 15 % of initial concentration of CNTs.

The capacitive effects were studied using CV and EIS. According to a power law equation

$$I = a \, \upsilon^b$$

This equation can be rearranged into following form

$$\log I \quad = \log a \, \upsilon^b$$

$$= \log a + b\log \upsilon$$

$$b \quad = \frac{\log I - \log a}{\log \upsilon}$$

$$\frac{\log I}{\log \upsilon} \quad = b + \log \upsilon^a$$

The intercept and slope of the graph $\log \upsilon$ vs log *I* can reveal the values of *a* and *b.* Value of *b* in this equation provides useful information about the charge storage mechanism. If current is

controlled by semi-infinite linear diffusion processes the value of *b* would be 0.5 and the above equation can be written as: $I = av^{1/2}$. If the value of *b* equals 1 the kinetics of electrode are controlled by surface redox reactions and are capacitive in nature. In this case the equation 1 can be written as $I = C_d A\ \upsilon$

Additional note:

The surface area plays an important role in energy storage through capacitive processes. Since capacitive effect arises due to the surface or near surface reactions it can be understood that higher surface area may lead to the higher energy storage. This need to be studied further in case of lithium ion batteries. Also combining porosity with surface area improves the electrode kinetics significantly. Which is significant from our results. It is also interesting to note that in case of AQ COF@CNTs, the synergetic effect of CNTs and COFs lead to significant increase in the surface area of composite. This is again an important insight which shows that CNTs are not only acting as an agent to improve the conductivity but they can also improve the structural aspects of the COF in our case**.**
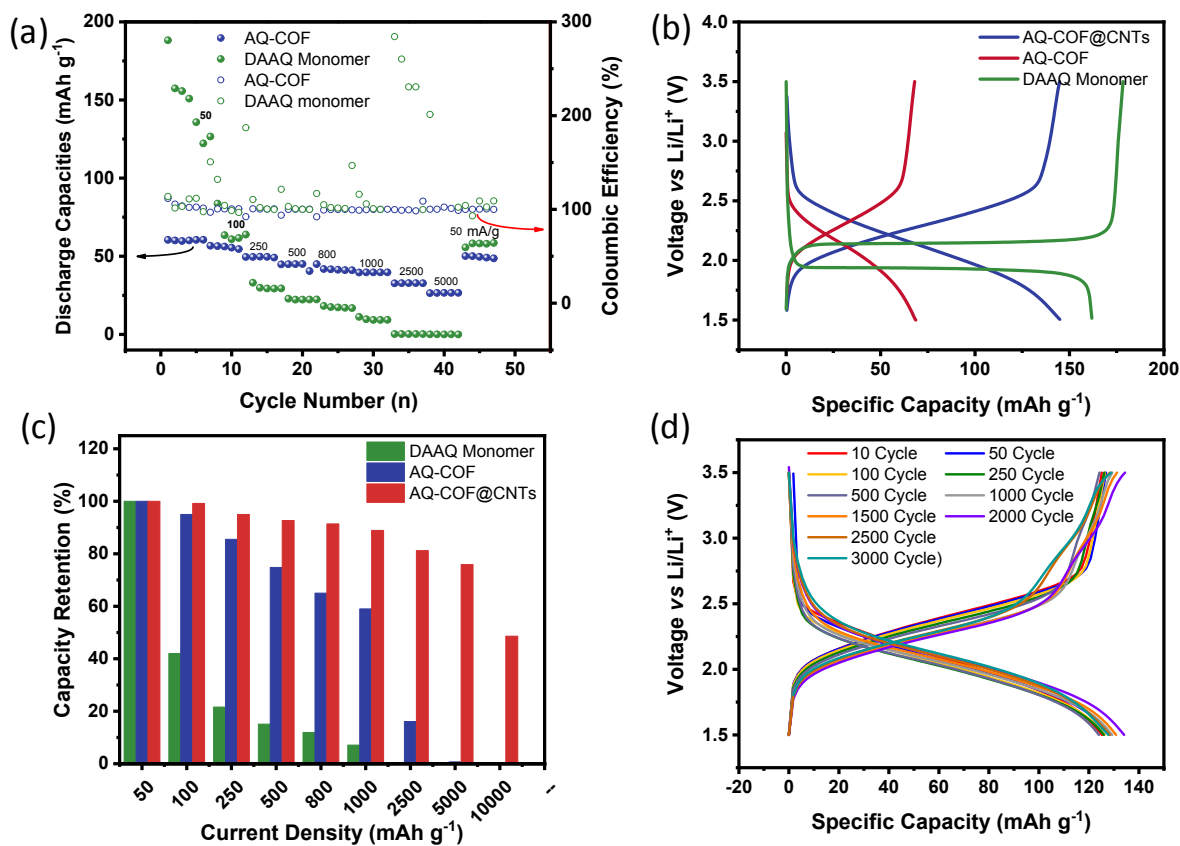
Figure S9: (a) Comparison of charge discharge performance with DAAQ monomer along with coulombic efficiency. (b) charge discharge curves. A horizontal plateau was observed for DAAQ monomer but a steep plateau was observed in case of both products which is an indication of capacitive effect. (c) percentage of capacity retention at different current densities. Charged discharged curves for long term cyclic performance at different cycles.
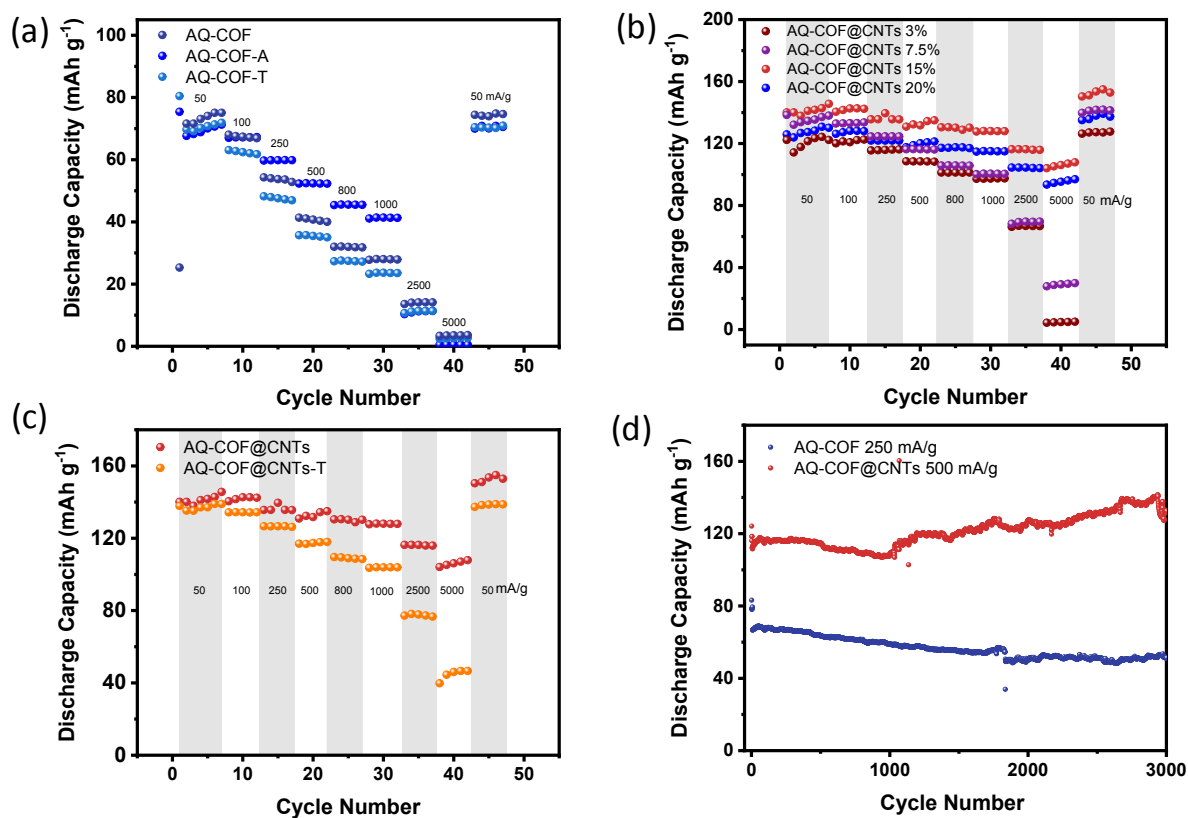
Figure S10: (a) Charge discharge performance of AQ COF synthesized at different conditions. (b) Charge discharge performance of AQ COF@CNTs with different ratio of CNTs. (c) Performance comparison of AQ COF@CNTs grown in different conditions. The lower capacity is due to bad dispersion of CNTs in glass tube method which is exhibited by SEM results. (d) long term cyclic performance of AQ COF at 250 mA/g and AQ COF@CNTs at 500 mA/g.
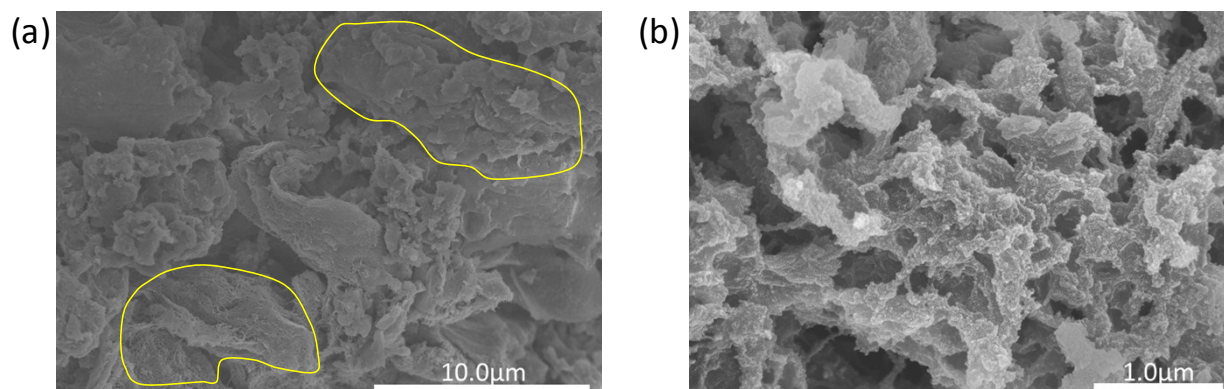
Figure S11: We were unable to obtained a uniformly dispersed CNTs into the reactant mixture while suing the glass tube as reaction vial. As a result, we found isolated bundles of CNTs and AQ COF instead of uniform growth of AQ COF on CNTs. This might be one reason for poor capacity in AQ COF@CNTs T.
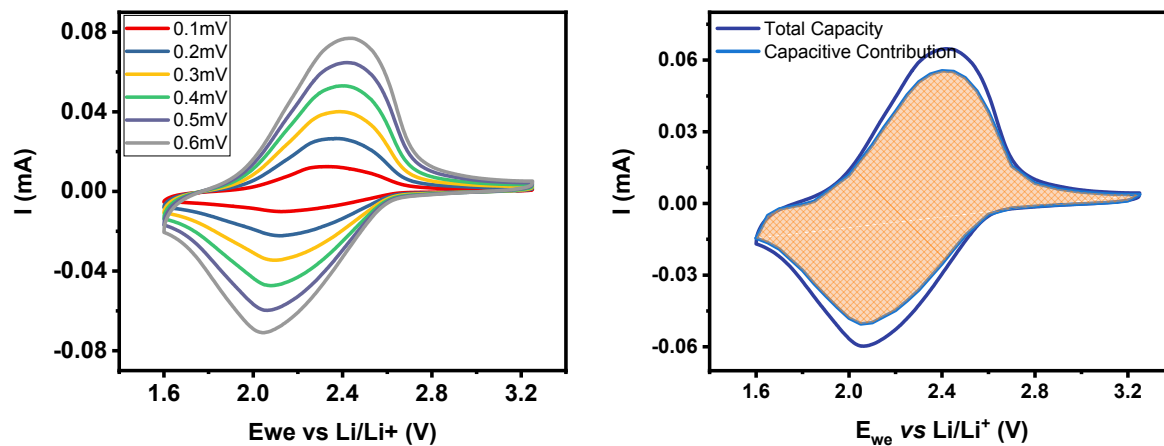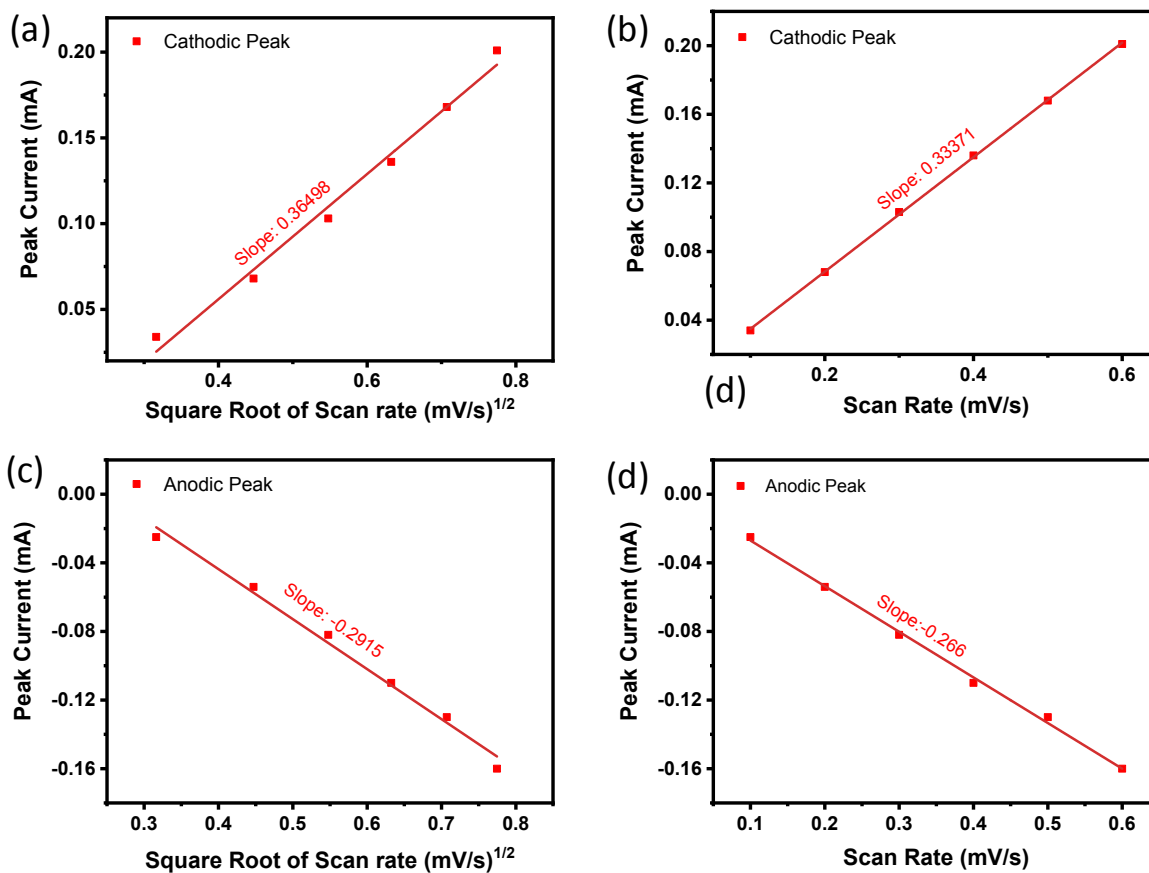

Figure S12: (a) CV at different scan rates of COF-A, (b) capacitive contribution in total capacity at 0.5 mV/s
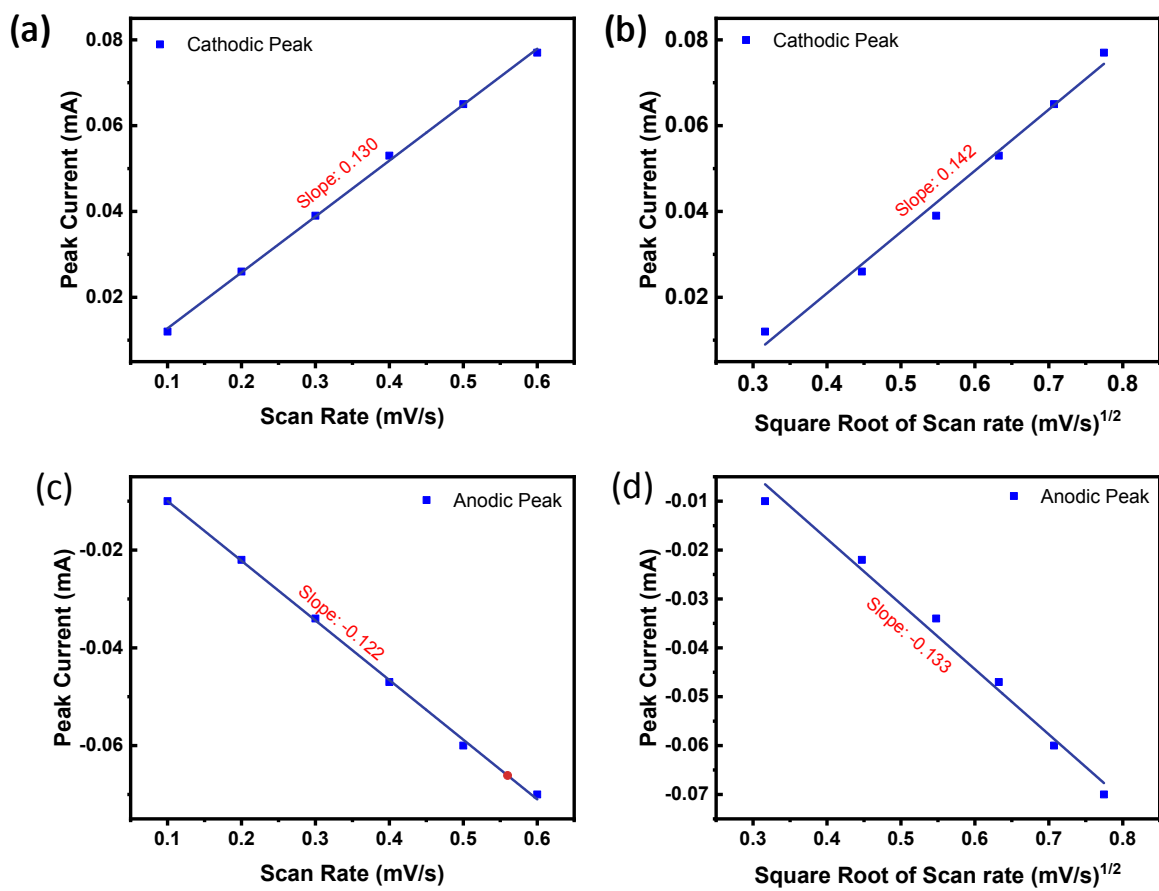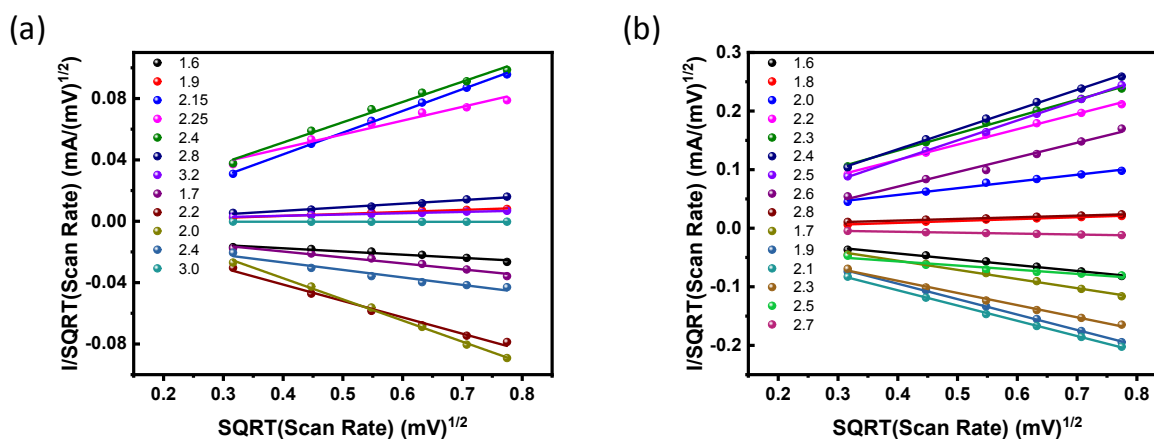
Figure S13: Relationship of scan rate and square root of scan rate with peak current for AQ COF for both cathodic and anodic peaks

Figure S14: Relationship of scan rate and square root of scan rate with peak current for AQ COF@CNTs for both cathodic and anodic peaks

Figure S15: Calculation of some of constants k_1 and k_2 at given potential for (a) AQ COF and (b) AQ COF@CNTs to determine the capacitive and diffusion-controlled capacity contribution. Slopes and intercept are calculated at different potential.
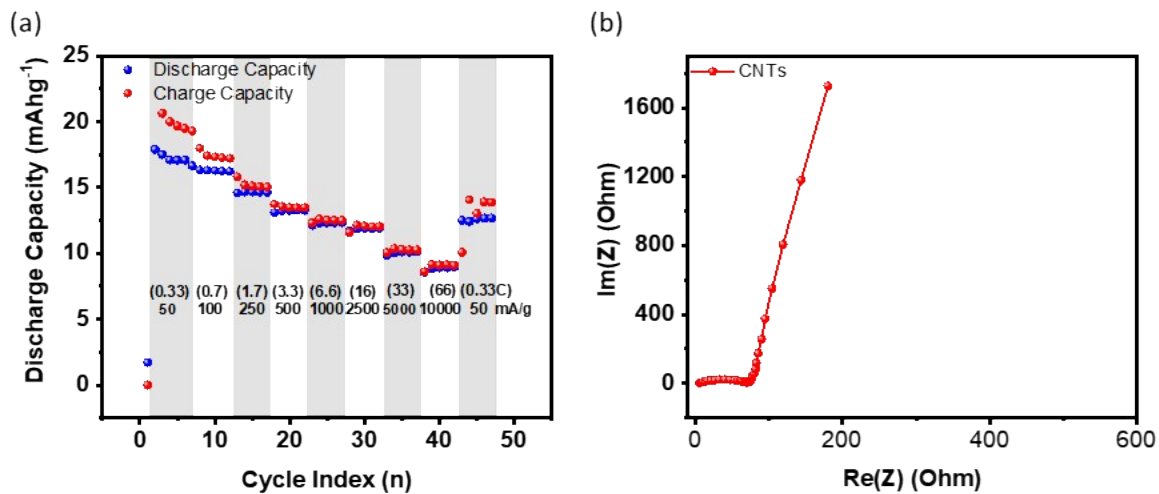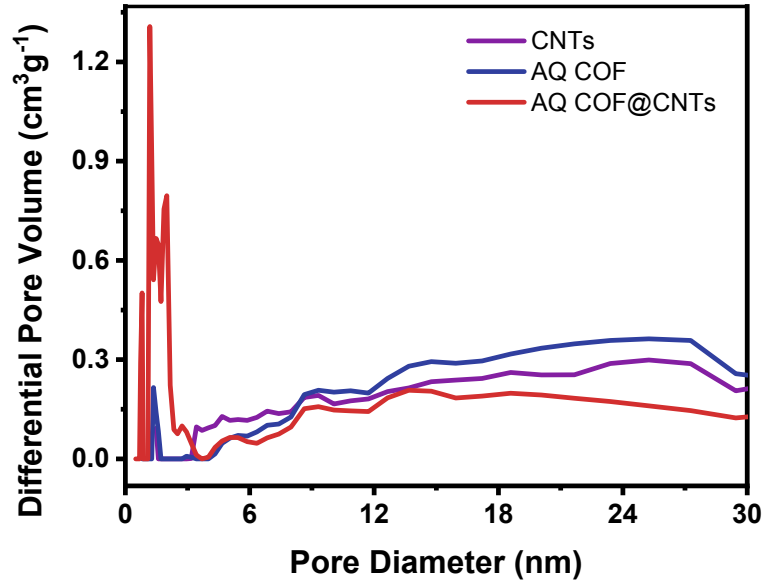
Figure S16: Charge and discharge capacity of pure CNTs cell with 60 %CNTs, 30% conductive carbon and 10% binder. (b) The EIS measurement for pure CNTs device.

Figure S16: Charge and discharge capacity of pure CNTs cell with 60 %CNTs, 30% conductive carbon and 10% binder. (b) The EIS measurement for pure CNTs device.

Figure S17: Pore size distribution of CNTs, AQ COF and AQ COF@CNTs

Table S1: Comparison of rate and cyclic Performance with some of published results

Cathode Material	Electrode Composition (AM: CC: B)	Maximum C rate (C), Capacity Retention (%)	C rate, Number of Cycles	Capacity Retention (%)	Reference
DAAQ-ECOF	6:3:1	19.9C, 50	3.3C, 1800	98	[1]
PIBN-G	8:1:1	10C, 71	1C, 300	86	[5]
C-LFP/C-PPy hybrid gel framework		30C, 40	1C, 500	75	[6]
YPTPA	3:5:4	18.3C, 92	NA, 1700	91.4	[7]
DTP-ANDI-COF @CNTs	6:2:2	12C, 85	2.4C, 700	100	[8]
PI10G	6:3:1	5, 68C.7	5C, 1000	89	[9]
Tb-DANT-COF	6:2:2	14.9C, 63	3.4C, 300	76.2	[10]
PDHBQS	7:3:0	15.8C, 41	0.79C, 500	89	[11]
AQ COF@CNTs	**6:3:1**	**66C, 48**	**1.7C, 3000**	**100**	**This Work**

AM: Active Material, CC: Conductive Carbon, B, Binder

Table S2: Comparison of diffusion ion constant values with some published results

Material	D_{Li+} (cm^2s^{-1})	Reference
DAAQ-ECOF	6.94×10^{-11}	[1]
LiFePO$_4$/C	1.64×10^{-14}	[12]
LiFePO$_4$/C-LaPO$_4$ (4.0 mol%)	4.0×10^{-13}	[12]
Li$_3$V$_2$(PO$_4$)$_3$	1.5×10^{-11}	[13]
TiNb$_6$O$_{17}$	3.72×10^{-13}	[14]
Nano Silicon	5.1×10^{-12}	[15]
LiCoO$_2$	$10^{-13} – 10^{-12}$	[16]
AQ COF	7.35953 x $10^{-12}cm^2s^{-1}$	**This work**
AQ COF@CNTs	1.87148 x10^{-10} cm^2s^{-1}	**This Work**

Table S3: Summary of The BET surface area and porosity measurement.

Material	BET Surface Area (m^{2}g^{-1})	Pores Volume (cm^{3}g^{-1})	Micropores Volume (cm^{3}g^{-1})	Pore Size (nm)
CNTs	212.3	0.36	0.028	6.7
AQ COF	231.4	0.35	0.05	1.35, 9.3
AQ COF@CNTs	905.3	0.82	0.27	1.2, 2.0

1. S. Wang, Q. Wang, P. Shao, Y. Han, X. Gao, L. Ma, S. Yuan, X. Ma, J. Zhou, X. Feng and B. Wang, *J. Am. Chem. Soc.*, 2017, **139**, 4258-4261.
2. J. H. Chong, M. Sauer, B. O. Patrick and M. J. MacLachlan, *Org. Lett.*, 2003, **5**, 3823-3826.
3. C. R. DeBlase, K. E. Silberstein, T. T. Truong, H. D. Abruna and W. R. Dichtel, *J. Am. Chem. Soc.*, 2013, **135**, 16821-16824.
4. K. Amin, L. Mao and Z. Wei, *Macromol. Rapid Commun.*, 2018, DOI: 10.1002/marc.201800565, e1800565.
5. Z. Luo, L. Liu, J. Ning, K. Lei, Y. Lu, F. Li and J. Chen, *Angew. Chem. Int. Ed. Engl.*, 2018, DOI: 10.1002/anie.201805540.
6. Y. Shi, X. Zhou, J. Zhang, A. M. Bruck, A. C. Bond, A. C. Marschilok, K. J. Takeuchi, E. S. Takeuchi and G. Yu, *Nano Lett.*, 2017, **17**, 1906-1914.
7. C. Zhang, X. Yang, W. Ren, Y. Wang, F. Su and J.-X. Jiang, *J. Power Sources*, 2016, **317**, 49-56.
8. F. Xu, S. Jin, H. Zhong, D. Wu, X. Yang, X. Chen, H. Wei, R. Fu and D. Jiang, *Sci. Rep.*, 2015, **5**, 8225.
9. H. Lyu, P. Li, J. Liu, S. Mahurin, J. Chen, D. K. Hensley, G. M. Veith, Z. Guo, S. Dai and X.-G. Sun, *Chemsuschem*, 2018, **11**, 763-772.
10. D.-H. Yang, Z.-Q. Yao, D. Wu, Y.-H. Zhang, Z. Zhou and X.-H. Bu, *J. Mater. Chem. A*, 2016, **4**, 18621-18627.
11. K. Amin, Q. Meng, A. Ahmad, M. Cheng, M. Zhang, L. Mao, K. Lu and Z. Wei, *Adv. Mater.*, 2018, **30**.
12. Z. Ma, Y. Peng, G. Wang, Y. Fan, J. Song, T. Liu, X. Qin and G. Shao, *Electrochim. Acta*, 2015, **156**, 77-85.
13. X. H. Rui, N. Ding, J. Liu, C. Li and C. H. Chen, *Electrochim. Acta*, 2010, **55**, 2384-2390.
14. Y. S. Lee and K. S. Ryu, *Sci. Rep.*, 2017, **7**, 16617.
15. N. Ding, J. Xu, Y. X. Yao, G. Wegner, X. Fang, C. H. Chen and I. Lieberwirth, *Solid State Ionics*, 2009, **180**, 222-225.
16. C. Chen, A. Buysman, E. Kelder and J. Schoonman, *Solid State Ionics*, 1995, **80**, 1-4.